TU Delft

Delft University of Technology

Gene-Directed FtsZ Ring Assembly Generates Constricted Liposomes with Stable Membrane Necks

Godino, Elisa; Danelon, Christophe

DOI
10.1002/adbi.202200172

Publication date
2023

Document Version
Final published version

Published in
Advanced Biology

Citation (APA)
Godino, E., & Danelon, C. (2023). Gene-Directed FtsZ Ring Assembly Generates Constricted Liposomes with Stable Membrane Necks. *Advanced Biology*, *7*(3), Article 2200172. https://doi.org/10.1002/adbi.202200172

Important note
To cite this publication, please use the final published version (if applicable).
Please check the document version above.

Copyright
Other than for strictly personal use, it is not permitted to download, forward or distribute the text or part of it, without the consent of the author(s) and/or copyright holder(s), unless the work is under an open content license such as Creative Commons.

Takedown policy
Please contact us and provide details if you believe this document breaches copyrights.
We will remove access to the work immediately and investigate your claim.

This work is downloaded from Delft University of Technology.
For technical reasons the number of authors shown on this cover page is limited to a maximum of 10.

ADVANCED BIOLOGY
www.advanced-bio.com

Gene-Directed FtsZ Ring Assembly Generates Constricted Liposomes with Stable Membrane Necks

*Elisa Godino and Christophe Danelon**

Mimicking bacterial cell division in well-defined cell-free systems has the potential to elucidate the minimal set of proteins required for cytoskeletal formation, membrane constriction, and final abscission. Membrane-anchored FtsZ polymers are often regarded as a sufficient system to realize this chain of events. By using purified FtsZ and its membrane-binding protein FtsA or the gain-of-function mutant FtsA* expressed in PURE (Protein synthesis Using Reconstituted Elements) from a DNA template, it is shown in this study that cytoskeletal structures are formed, and yield constricted liposomes exhibiting various morphologies. However, the resulting buds remain attached to the parental liposome by a narrow membrane neck. No division events can be monitored even after long-time tracking by fluorescence microscopy, nor when the osmolarity of the external solution is increased. The results provide evidence that reconstituted FtsA-FtsZ proto-rings coating the membrane necks are too stable to enable abscission. The prospect of combining a DNA-encoded FtsZ system with assisting mechanisms to achieve synthetic cell division is discussed.

1. Introduction

Synthetic cell research has become a rapidly growing field in synthetic biology and is rooted to the concept of "minimal cell" coined by Luisi and co-workers.[1–4] The ultimate goal is to create an entire living cell from the ground up using a minimal set of biological and chemical building blocks. The reconstitution of DNA-encoded protein systems offers a route toward autocatalysis of the network's constituents and, eventually, autonomous replication of the evolutionary compartment.

A starting point to establish compartmental division, a hallmark of cellular life, in cell-free systems, is to identify the main components and processes involved in bacterial cytokinesis and to reconstitute them in vitro, most relevantly inside lipid vesicles. With a limited number of division factors compared to eukaryotes, the *Escherichia coli* divisome has been at the center of numerous efforts attempting to split liposomes.[5–12] In vivo, a contractile ring composed of FtsZ, FtsA, and ZipA is formed at midcell.[13,14] FtsZ is a bacterial homologue of tubulin[15–17] that polymerizes into self-interacting filaments when bound to GTP.[18–21] FtsZ lacks a membrane targeting domain, and it is anchored to the cytoplasmic bilayer by FtsA and ZipA.

In vitro reconstruction of FtsZ polymers,[15,22] FtsA and ZipA[23] in model membranes has contributed to elucidate the self-organization and dynamics of the *E. coli* division proteins. In 2008, Osawa and colleagues suggested that Z-rings could generate constriction forces within tubular liposomes in the absence of motor proteins.[5] In this work, FtsZ-mts (a chimeric FtsZ with a membrane targeting sequence fused to the C terminus) caused membrane invagination, though full constriction was not achieved.[5] The authors proposed that the conformational change of FtsZ from straight to curved filaments acts as the driving force. In a follow-up study, the same group claimed that the Z-ring stimulates membrane constriction in giant liposomes to the point of septation.[7] The use of FtsA*, a gain-of-function mutant of FtsA,[24] was required to achieve complete scission, as such division events were not observed with FtsZ-mts. Szwedziak and colleagues showed that purified FtsZ and FtsA from *Thermotoga maritima* form continuous filament rings encircling the membrane on the inside of small unilamellar vesicles, generating constriction sites but evidences of membrane abscission were not presented.[9] The authors proposed a scenario, where the sliding and shortening of overlapping FtsZ filaments constitute the main force generator.[9] Interestingly, Ramirez Diaz and colleagues reported that FtsZ filaments do not have a single curvature,[25] and that their intrinsic helical structure drives liposome deformation via torsional stress, a mechanism that is reliant on GTP hydrolysis.[12] With the aim to recapitulate a functional Z-ring from gene-encoded proteins in liposomes, our group has demonstrated that ring-like cytoskeletal structures led to membrane constriction into narrow necks connecting budding vesicles,[11] a phenotype that differs from that observed in previous studies by the more pronounced pinching of the liposome membrane. Although no division events could unambiguously be detected, our experimental design was not directed toward addressing

E. Godino, C. Danelon
Department of Bionanoscience
Kavli Institute of Nanoscience
Delft University of Technology
Delft 2629HZ, The Netherlands
E-mail: c.j.a.danelon@tudelft.nl

The ORCID identification number(s) for the author(s) of this article can be found under https://doi.org/10.1002/adbi.202200172.

© 2023 The Authors. Advanced Biology published by Wiley-VCH GmbH. This is an open access article under the terms of the Creative Commons Attribution License, which permits use, distribution and reproduction in any medium, provided the original work is properly cited.

DOI: 10.1002/adbi.202200172

27010198, 0, Downloaded from https://onlinelibrary.wiley.com/doi/10.1002/adbi.202200172 by Tu Delft, Wiley Online Library on [09/01/2023]. See the Terms and Conditions (https://onlinelibrary.wiley.com/terms-and-conditions) on Wiley Online Library for rules of use; OA articles are governed by the applicable Creative Commons License

this specific question. Hence, the capability of membrane-tethered FtsZ to split liposomes remains open to discussion, both as a fundamental aspect in bacterial cytokinesis and as an implementation strategy for synthetic cell division.

Herein, we explore this question by coupling the assembly of Z-ring to cell-free protein synthesis with PURE system[26,27] inside liposomes. Specifically, we ask: Is the combination of FtsA and FtsZ sufficient to drive liposome division? Is FtsA* required for full septation? Can osmolarity differential across the liposome bilayer encourage fission of the FtsZ-constricted membrane neck? Time-lapse fluorescence imaging and quantitative analysis reveal distinct features between FtsA- and FtsA*-induced membrane constriction sites and bud morphologies. Yet, no evidences for septation or membrane neck splitting were found, suggesting that Z-ring stability is the bottleneck for division. We finally discuss experimental approaches to enable Z-ring-constricted liposomes to undergoing actual division.

2. Results

2.1. Quantitative Analysis of FtsA-FtsZ-Mediated Liposome Constriction Sites

We performed reconstitution experiments of gene-encoded FtsA-FtsZ cytoskeletal structures in liposomes (**Figure 1**a). Compared to our previous work,[11] we optimized the protocol to increase the occurrence of liposomes exhibiting constriction sites and budding vesicles, allowing us to perform statistical analysis of the different morphological features (Experimental Section). Recruitment of the fluorescently labeled FtsZ-Alexa647 (FtsZ-A647) to the liposome membrane was detectable within 1.5 h of expression, while shape deformations in the form of protrusions or membrane necks connecting budding vesicles to the parental liposome were only observed after 2–3 h (Figure 1b,c and Figure S1a, Supporting Information). About 45% of liposomes display membrane deformation (including in the form of short protrusions) and ≈18% of total liposomes exhibit neck formation. These values are likely underestimated since membranous structures may be located outside the imaging plane. Importantly, membrane remodeling events can clearly be attributed to FtsZ clusters as such structures do not appear when FtsA is not expressed (Figure S1b, Supporting Information). The FtsZ-coated membrane necks generally span over a few micrometers, forming a tubular structure with an apparent length of 1.5 ± 0.8 μm (over 50 constriction sites analyzed across three biological replicates) (Figure 1d). No correlation was found between the size of the parental liposome and the length of the neck (Figure 1d). The tethered budding vesicles have an apparent (and most likely underestimated) diameter of 2.2 ± 0.8 μm (over 50 buds analyzed across three biological replicates) (Figure 1e). Interestingly, some liposomes exhibit a dumbbell-shape geometry consisting of two almost equally sized liposomes connected by a membrane neck. Moreover, we observed that multiple necks with blebs can develop from a single mother liposome (Figure 1f,g), representing about 44% of the total number of constricted liposomes. Up to four necks with tethered vesicles may originate from one liposome, and buds can either be arranged one after another in a pearling like manner or connected via a branching point (Figure 1g). We repeated the assay several times with our standard lipid composition and with only DOPG-DOPC lipids, with different batches of lipids, DNA templates, PURE system, and purified FtsZ-A647. All results were consistent across the tested conditions, demonstrating the robustness of our protocol to generating constricted liposomes by genetic control of Z-ring protein assembly.

2.2. Timelapse Imaging of Constricted Liposomes Did Not Reveal Division Events

We then set out to examine how constricted liposomes form and develop using time-lapse confocal microscopy. In particular, liposomes were tracked over time to determine whether division events might occur by closure of the membrane neck in the form of a septum or detachment of the buds. Over 50 liposomes with varying numbers of necks and blebs were imaged every 10 s for a duration of a few minutes up to 40 min (**Figure 2**a). The exact duration depended on how fast the liposomal structures were moving and our ability to maintain them in focus. None of the imaged liposomes underwent visible division. Despite clear dynamics, the membrane necks are stable and the buds permanently attached regardless of the liposomal phenotypes. This result indicates that, in the studied conditions, FtsA-FtsZ is capable of constricting liposomes into narrow membrane necks but is not sufficient to complete abscission. We cannot exclude that small blebs (<1 μm in diameter) may have been expelled from the parental liposome from out-of-focus planes. Recording such fast events would technically be challenging. We found that some of the FtsA-FtsZ clusters were dynamic and could slide along the membrane necks. Moreover, we observed in a few liposomes that opposite membrane sites were pinching, presumably because of the condensation of FtsZ polymers (Figure 2b and Figure S1c, Supporting Information).

2.3. Inward Membrane Invaginations Produced by Extraliposomal Assembly of FtsA-FtsZ Polymers

To better visualize the membrane remodeling events and, possibly, catch the release of budding vesicles, we produced FtsA-anchored FtsZ filaments from the outside of liposomes (**Figure 3**a). After 1 h, we observed that FtsZ was recruited on the outside of the liposomes and was drilling concave deformations into the membrane (Figure S2, Supporting Information). As the expression of FtsA continued, multiple inward tubular membranous structures partly or entirely coated with FtsZ were detected (Figure 3b–d). These membrane invaginations spanned several micrometers, could display terminating buds and developed irrespective of the liposome size (Figure 3b–d). Some of the budding vesicles can be several micrometers in diameter (Figure 3c) and, in large liposomes (diameter typically >5 μm), densely packed invaginated membrane structures with multiple necks, branching points and buds can accumulate (Figure 3d). The fact that FtsA-FtsZ clusters at a constriction site can split, resulting in multiple necks connected with

© 2023 The Authors. Advanced Biology published by Wiley-VCH GmbH

27010198, 0, Downloaded from https://onlinelibrary.wiley.com/doi/10.1002/adbi.202200172 by Tu Delft, Wiley Online Library on [09/01/2023]. See the Terms and Conditions (https://onlinelibrary.wiley.com/terms-and-conditions) on Wiley Online Library for rules of use; OA articles are governed by the applicable Creative Commons License

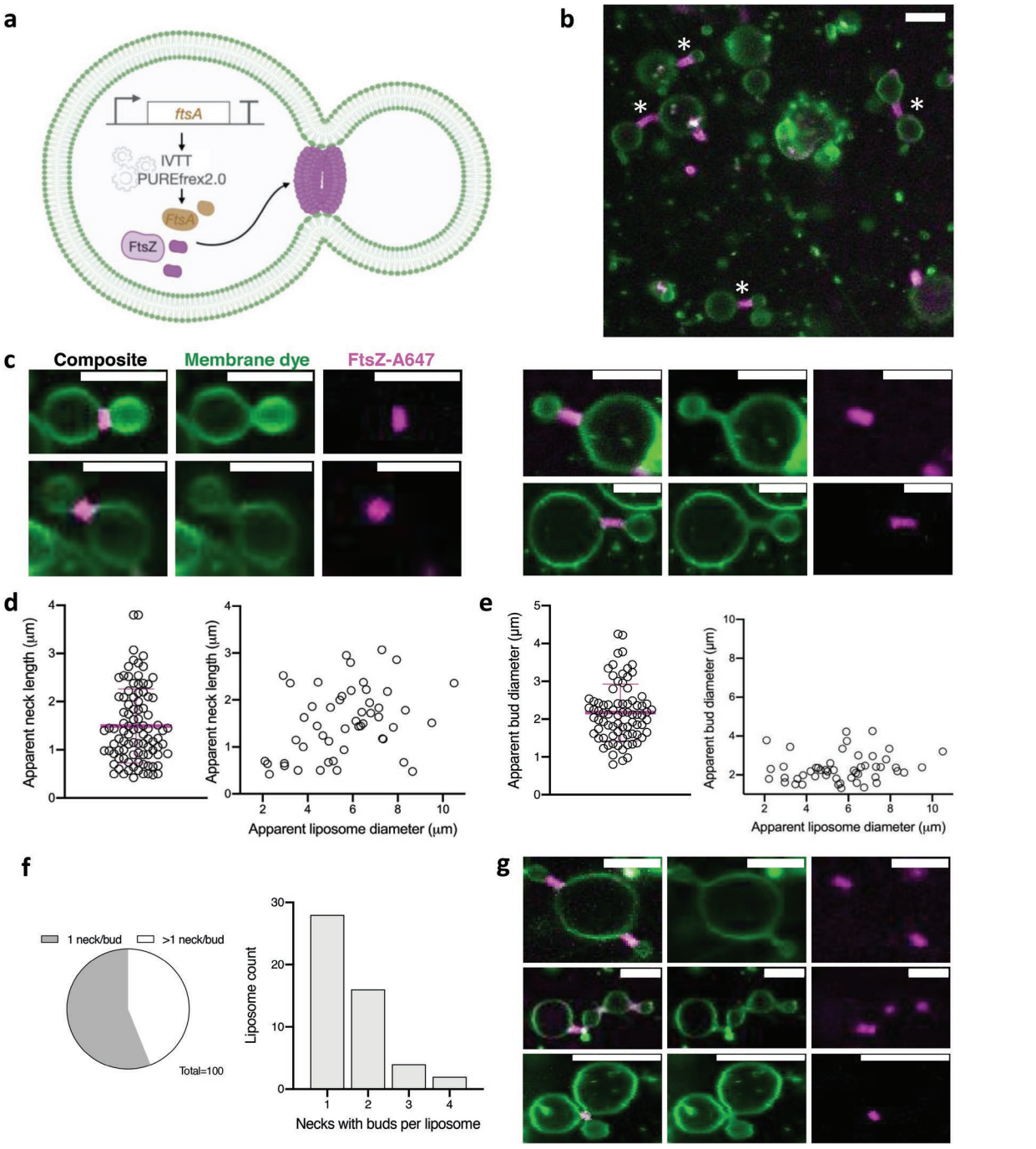

Figure 1. Quantitative analysis of the liposome phenotypes induced by gene-encoded FtsA-FtsZ contractile rings. a) Schematic illustration of the liposome reconstitution assay. The *ftsA* gene was cell-free expressed within phospholipid vesicles in the presence of 3×10^{-6} M purified FtsZ-A647. IVTT, in vitro transcription-translation. b) Confocal fluorescence image showing liposomes with constricted membrane sites colocalizing with expressed FtsA-FtsZ clusters. Asterisks indicate FtsA-FtsZ-coated membrane necks connecting budding vesicles. c) Confocal fluorescence images of individual liposomes exhibiting representative phenotypes. The membrane neck can be shorter (left) or longer (right) than 1 μm. d) The length of the membrane necks was analyzed. Images of the parental liposomes ($n = 50$) were acquired near the equatorial plane to calculate the apparent diameter. No correlation was observed between the liposome size and neck extension. The mean value and standard deviation are appended in magenta. e) The diameter of the buds and of the parental liposomes ($n = 50$) were measured near their equatorial plane. In (d) and (e) the mean value and standard deviation are appended in magenta. f) Analysis of the number of necks/buds produced per liposome ($n = 50$). The number of necks ranges from 1 to 4, with 44% of the parental liposomes featuring more than one. Considering the fast motion of these lipidic structures, it is possible that these values are slightly underestimated. g) Confocal fluorescence images showing the dominant morphologies of liposomes exhibiting buds with multiple necks: unconnected protrusions terminated with a budding vesicle (top), liposome pearling corresponding to connected buds by a membrane neck (middle), and multiple buds connected through a branching point (bottom). The membrane dye is displayed in green and FtsZ-A647 in magenta. The composite image is the overlay of the two channels. Scale bars are 5 μm.

© 2023 The Authors. Advanced Biology published by Wiley-VCH GmbH

27010198, 0, Downloaded from https://onlinelibrary.wiley.com/doi/10.1002/adbi.202200172 by Tu Delft, Wiley Online Library on [09/01/2023]. See the Terms and Conditions (https://onlinelibrary.wiley.com/terms-and-conditions) on Wiley Online Library for rules of use; OA articles are governed by the applicable Creative Commons License

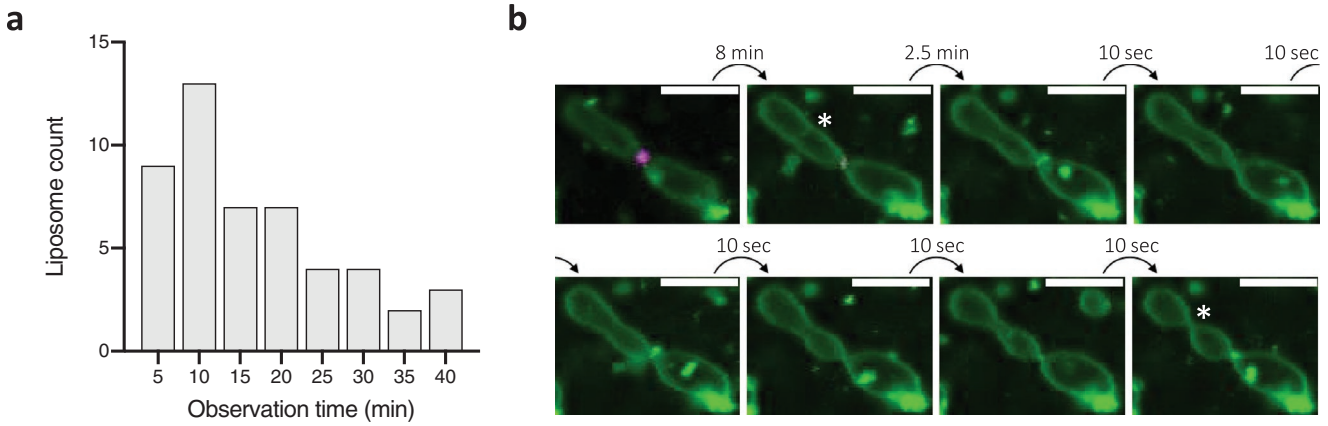

Figure 2. Temporal analysis of constricted liposomes. a) The graph reports the number of liposomes with FtsZ-colocalizing membrane necks and blebs that were imaged every 10 s over a certain time span, from a few minutes to 40 min. None of the studied liposomes underwent division during the observation period. b) Time sequence images showing the appearance of a constriction site (indicated with an asterisk in the second and last frames) in the course of time. The corresponding FtsZ-A647 fluorescent signal is not visible due to photobleaching during the first 8 min of imaging. The time lapse between consecutive images is appended. The membrane dye is colored in green and FtsZ-A647 in magenta. The displayed composite image is the overlay of the two channels. Scale bars are 5 μm.

blebbing vesicles,[11] may explain this phenomenon. We carefully inspected the numerous inner vesicles over time and by scanning different imaging planes to assess whether they were tethered to the parental liposome or free-floating in the lumen. We gathered that none of the inward membrane protrusions matured into division events, confirming the observations made from internally produced FtsA-FtsZ filaments (Figure 1).

2.4. Osmotic Deflation Causes Drastic Membrane Remodeling and Z-Ring Disassembly

Osmotically deflated liposomes are particularly prone to membrane remodeling in the presence of division players.[28] Our present findings suggest that the stability of constricted Z-rings precludes membrane neck splitting and may constitute

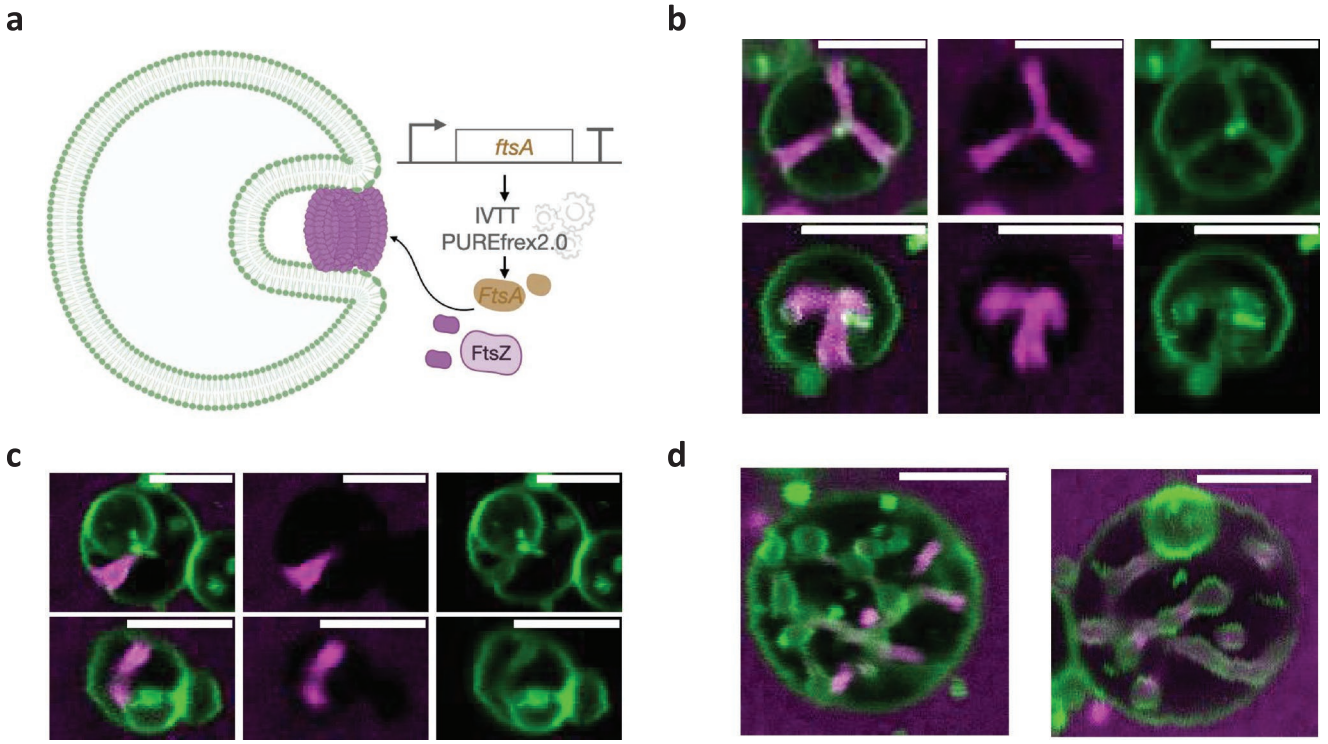

Figure 3. Characterization of membrane shape transformations induced by FtsA-FtsZ filaments generated at the exterior of liposomes. a) Schematic illustration of the inside-out liposome reconstitution assays, where the *ftsA* gene and 3×10^{-6} M purified FtsZ-A647 were supplemented in the outer liposome solution. b–d) Confocal fluorescence images of liposomes exhibiting inward tubulations entirely coated with FtsZ, a large budding vesicle, and numerous invaginated membrane structures pinched off by visible FtsZ clusters, respectively. The membrane dye is colored in green and FtsZ-A647 is in magenta. The composite image is the overlay of the two channels. Scale bars are 5 μm.

© 2023 The Authors. Advanced Biology published by Wiley-VCH GmbH

27010198, 0, Downloaded from https://onlinelibrary.wiley.com/doi/10.1002/adbi.202200172 by Tu Delft, Wiley Online Library on [09/01/2023]. See the Terms and Conditions (https://onlinelibrary.wiley.com/terms-and-conditions) on Wiley Online Library for rules of use; OA articles are governed by the applicable Creative Commons License

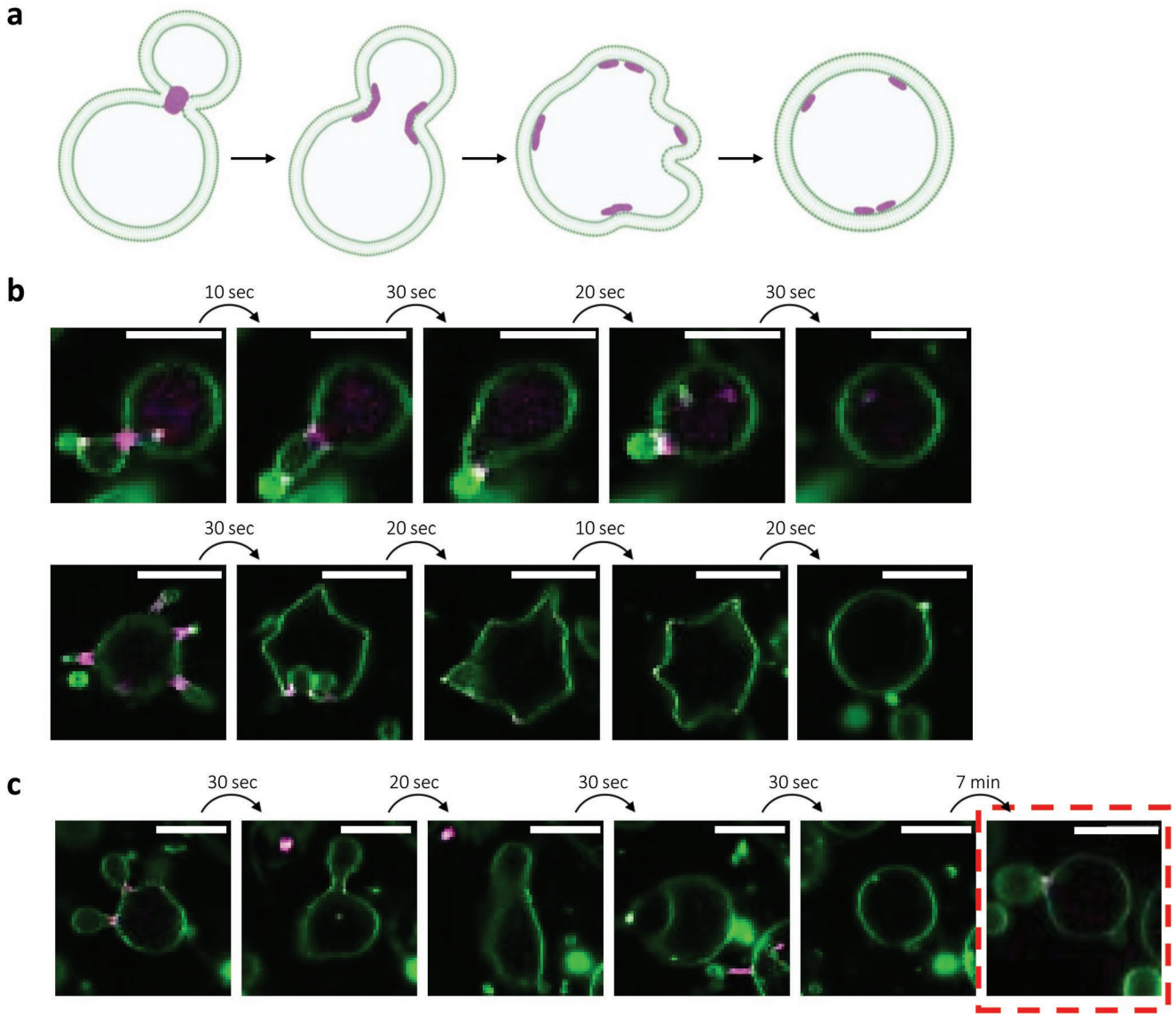

Figure 4. Fate of Z-ring-mediated constriction sites in osmotically deflated liposomes. a) Schematic illustration of liposome shape transformation and Z-ring disassembly (colored in magenta) upon external addition of sucrose. b) Time series images of three constricted liposomes (first row) exposed to an external differential of 100×10^{-3} M sucrose. Upon osmotic shock, membrane neck destabilization is followed by extensive remodeling during which liposomes incorporate the excess membrane and resume into a spherical shape. c) As in (b) but here the liposome assumed a rounded shape and later developed constricting necks again (last frame). The images are overlays of the membrane dye signal (green) and the FtsZ-A647 signal (magenta). Scale bars are 5 μm.

the bottleneck for dividing liposomes, not Z-ring formation nor constriction into narrow membrane tubes. We reasoned that membrane remodeling induced by an intense hypotonic shock (higher osmolarity outside than inside liposomes) may affect Z-ring stability, thus decreasing the energy barrier for the opposing bilayers to come closer and fuse. Alternatively, sudden membrane destabilization accompanied with a local increase of the spontaneous curvature at the neck region might be sufficient to trigger bilayer fusion events.

When adding 100×10^{-3} M sucrose to the outer solution of pre-constricted liposomes, a few of them showed an excess number of FtsZ-coated membrane necks and buds (Figure S3a, Supporting Information), while most liposomes underwent drastic membrane remodeling accompanied by Z-ring disassembly and relaxed back into a spherical shape (**Figure 4**a–c). Liposomes that have assumed a rounded shape as a result of sucrose-induced membrane remodeling can develop constricting necks over time (Figure 4c). It appears that membrane wobbling compromises the stability of FtsA-FtsZ structures, but instead of relaxing through neck splitting and release of the buds, large-scale fluctuations reshape liposomes into spheres, a process that must be associated to solvent or solute permeability across the membrane. When a greater concentration of sucrose (200×10^{-3} M) was applied to the external solution, the overall sample quality dropped and the remaining liposomes showed agglutinations of numerous membrane protrusions

© 2023 The Authors. Advanced Biology published by Wiley-VCH GmbH

27010198, 0, Downloaded from https://onlinelibrary.wiley.com/doi/10.1002/adbi.202200172 by Tu Delft, Wiley Online Library on [09/01/2023]. See the Terms and Conditions (https://onlinelibrary.wiley.com/terms-and-conditions) on Wiley Online Library for rules of use; OA articles are governed by the applicable Creative Commons License

and small vesicles (Figure S3b, Supporting Information). Together, sucrose-induced osmotic deflation of liposomes does not encourage division of FtsA-FtsZ-constricted liposomes.

2.5. Substituting FtsA with FtsA* Leads to Formation of Longer Membrane Protrusions Terminated by Smaller Buds

We then asked if the high stability of the protein rings and membrane necks was specific to the *E. coli* wild-type FtsA or if the gain-of-function mutant FtsA* (R286W)[24] could enable complete septation and division, as invoked in Osawa et al.[7] FtsA* has a reduced propensity to form oligomers which increases the packing density of FtsZ polymers compared to FtsA.[29,30] Therefore, we cell-free expressed FtsA* inside liposomes and reconstituted FtsA*-FtsZ cytoskeletal structures following the same protocol as described above (**Figure 5**a). Membrane recruitment of FtsZ in the form of patches was visible within 1.5 h of expression of FtsA* and major liposome-remodeling events were observed after 2 h (Figure 5b–d). In contrast to the type of structures formed with FtsA, the majority of the liposomes exhibited long and narrow outward membrane protrusions that were completely coated with FtsZ (Figure 5b). This result is in agreement with previous observations that FtsA* improves lateral interactions between FtsZ filaments and stabilizes FtsZ ring rearrangement.[29,30] Tubular protrusions had an apparent length of 3.2 ± 1.5 µm (n = 50 membrane tubes analyzed across three biological replicates, Figure 5c), which is about twofold longer than with the wild-type FtsA. No clear correlation was observed between the parental liposome

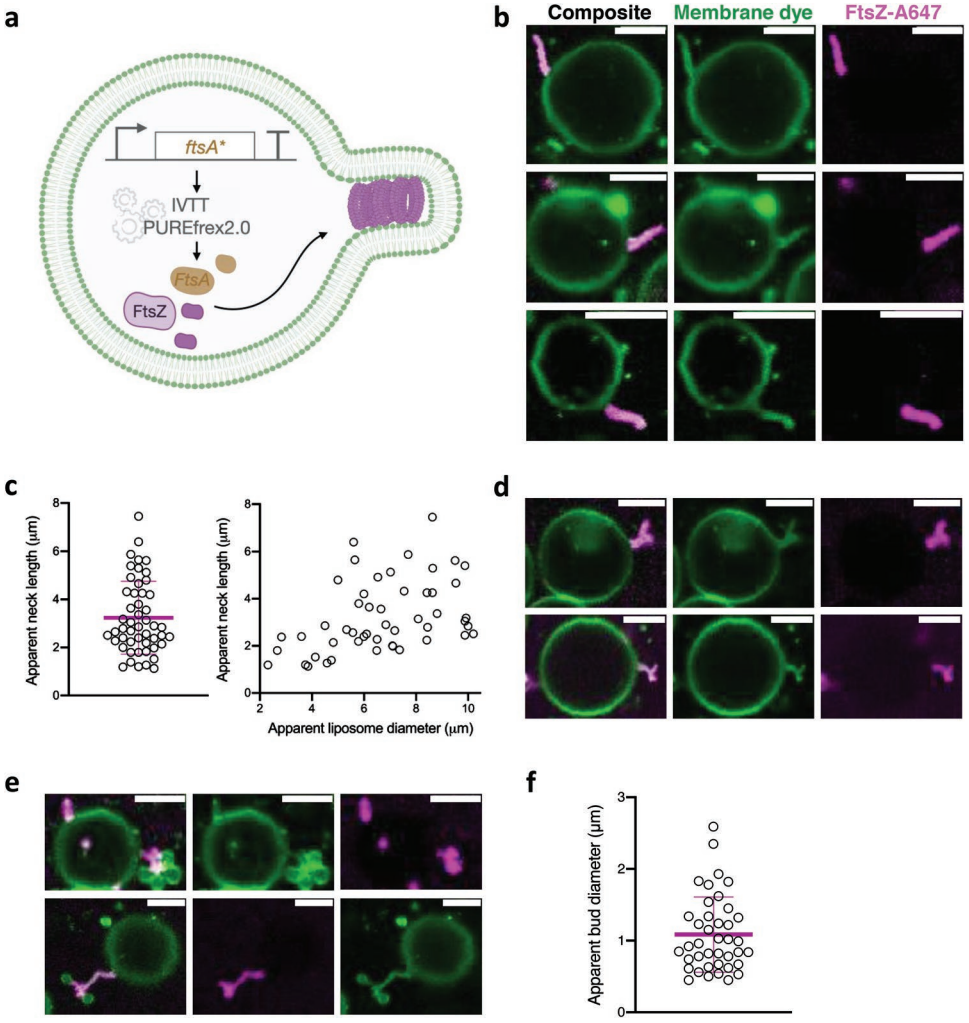

Figure 5. Cytoskeletal structures and membrane remodeling using the FtsA* mutant. a) Schematic illustration of the FtsA*-FtsZ-liposome assay. The *ftsA** gene was expressed within phospholipid vesicles in the presence of 3×10^{-6} M purified FtsZ-A647, as previously described with the wild-type gene. b) Confocal fluorescence images of liposomes exhibiting long and narrow outward membrane protrusions entirely coated with FtsZ. c) The length of these membrane extensions was quantified as described in Figure 1 (n = 50 liposomes analyzed). The appended magenta lines are the mean value and standard deviation. d) Confocal fluorescence images showing that long tubulated membranes can bifurcate into two or three branches. e) The extremity of the neck can bear a cluster of small vesicles. f) The apparent bud size was analyzed as described in Figure 1. The appended magenta lines represent the mean value and standard deviation. The membrane dye is colored in green and FtsZ-A647 is in magenta. The composite image is the overlay of the two channels. Scale bars are 5 µm.

© 2023 The Authors. Advanced Biology published by Wiley-VCH GmbH

27010198, 0, Downloaded from https://onlinelibrary.wiley.com/doi/10.1002/adbi.202200172 by Tu Delft, Wiley Online Library on [09/01/2023]. See the Terms and Conditions (https://onlinelibrary.wiley.com/terms-and-conditions) on Wiley Online Library for rules of use; OA articles are governed by the applicable Creative Commons License

size and the length of the membrane necks. The terminal part of the membrane tubes can bifurcate into two or three branches (Figure 5d). In some cases, small vesicles with a size of 1.1 ± 0.6 μm (mean ± standard deviation, n = 40 buds analyzed across three biological replicates) were attached, typically in a grape-like shape (Figure 5e,f). No events of budding vesicle detachment were observed. However, it should be noted that time-lapse imaging of the same buds was challenging due to their fast dynamics, large distance from the mother liposome, and small sizes. Other membrane remodeling morphologies, such as patches, small outward deformations, and short protrusions were also observed but their occurrence was low. The canonical phenotype observed with FtsA, i.e., large (diameter >1 μm) vesicles tethered to the parental liposome through a membrane neck, was rarely detected with FtsA* (Figure S4b, Supporting Information).

The concentration of expressed FtsA and FtsA* was estimated by cotranslational labeling and polyacrylamide gel analysis (Figure S4a, Supporting Information), indicating that both proteins are produced at similar amounts. Therefore, the differences in FtsZ rearrangement, and extended membrane necks and protrusions with FtsA* can unambiguously be ascribed to differences in protein properties.

Our results suggest that an FtsA*-based Z-ring is not a good candidate for synthetic cell division. The small size of the budding vesicles creates an extreme asymmetry, which compromises the balanced partitioning of the molecular contents and, thus, the viability of some synthetic cell daughters.

3. Discussion

Building upon our finding that the bacterial cell division proteins FtsA and FtsZ constrict gene-expressing liposomes,[11] we herein improved the methodology to collect a large data set using time-lapse fluorescence imaging under varying experimental conditions, which allowed us to identify various phenotypes and extract morphological parameters: membrane neck dimension, number and size of budding vesicles, and a lower bound for the lifetime of the constriction sites. Expression and membrane interaction of FtsA-FtsZ filaments from the outside of liposomes helped us reconstruct the sequence of events yielding neck formation and vesicle budding (Figure 3b): First, concave membrane depressions were formed, followed by deep invagination, which resulted in the extrusion of membrane tubules. The inward deformations are comparable to those observed when purified FtsZ-YFP-mts was added to the outside of liposomes.[6] FtsZ protofilaments generating a bending force on the membrane was suggested as a step leading to concave depressions.[5] According to a more recent study, the inward membrane protrusions would be caused by a corkscrew-like FtsZ helix with multiple curvature directions.[25] A follow-up study revealed that membrane tubulation is induced by torsional stress initiated by an intrinsic twist along the FtsZ filament, a process that is stimulated by GTPase activity.[12] Interestingly, we also noticed a less common deformation mechanism in which the membrane is pinched off, resulting in narrow neck formation (Figure 2b). This observation is more consistent with another proposed model in which FtsZ filaments wrapped around the liposome membrane slide, pulling the opposing membrane regions together.[9]

Although different types of mechanisms may cause liposomes to constrict, probably depending on the exact molecular composition and mechanical state of the membrane, torsional stress followed by tubular membrane extrusion seems the most prevalent scenario. Further quantitative biophysical studies are needed to determine the forces required to accomplish the scission of the membrane necks and the implication of FtsZ filament treadmilling. It should be noted that transitioning from a spherical liposome to a constricted vesicle with bud formation is possible only if an excess of membrane area (surface-to-volume ratio increases) is generated. Solvent permeability across the bilayer may lead to the volume reduction that is necessary to accommodate liposome shape transformation. This mechanism is plausible when considering that a fraction of liposomes is permeable to an ≈790 Da molecule.[31]

Combining with data obtained using the gain-of-function mutant FtsA*, our results indicate that expressed FtsA*/FtsA and FtsZ robustly form ring-like structures within liposomes, which leads to pronounced membrane deformation in the form of necks of various dimensions and budding vesicles. However, this two-protein system fails to trigger division events for all constriction sites that were tracked up to 40 min. The question arises whether division events could be possible under different FtsZ/FtsA protein concentrations or phospholipid compositions. Although we tested a limited number of bulk initial conditions, a broad range of absolute and relative amounts of encapsulated FtsZ and FtsA can be investigated around their physiological values within *one* liposome sample. Differences in protein concentrations are due to variations in the encapsulation efficiency of macromolecules in liposomes and to the heterogeneity in gene expression levels.[31] The range of FtsA and FtsZ concentrations should have been sufficient to explore various states of filament length and dynamics given the large population of vesicles. With our previous study,[11] we tested two lipid compositions, both containing dioleoyl phospholipids and reflecting the surface charge density of the *E. coli* inner membrane. Similar lipid compositions have extensively been used by other groups investigating FtsZ or other bacterial membrane associated processes in vitro, showing activity of the reconstituted protein systems. *E. coli* polar lipid extracts would offer a more realistic hydrocarbon chain variety in terms of length, (un)saturation and propanylation, but the yield of gene expressing vesicles is not as high as with our standard lipid mixtures. Together, our data suggest that an FtsA-FtsZ-based minimal mechanism is unlikely to drive synthetic cell division on its own. The reported example of septum closure to the point of division appears today to have been a rare event that does not reflect a robust mechanism.[7]

FtsZ has traditionally been viewed as the primary source of constrictive force in vivo.[32] However, there have been accumulated doubts over the past few years regarding the role of FtsZ in the final stage of cell division. Our failure to obtain full septation in vitro by FtsZ-FtsA is consistent with these observations of the Z-ring in vivo. In support of the idea that FtsZ is not the driving force behind division, it was found that the pace of septum closure in *E. coli* cytokinesis is resistant to several Z-ring disturbances,[33] including changes in FtsZ GTPase

© 2023 The Authors. Advanced Biology published by Wiley-VCH GmbH

27010198, 0, Downloaded from https://onlinelibrary.wiley.com/doi/10.1002/adbi.202200172 by Tu Delft, Wiley Online Library on [09/01/2023]. See the Terms and Conditions (https://onlinelibrary.wiley.com/terms-and-conditions) on Wiley Online Library for rules of use; OA articles are governed by the applicable Creative Commons License

activity, Z-ring density, and time of ring assembly. Furthermore, Söderström and Daley observed that FtsZ leaves the *E. coli* division site at a constriction width comprised between 0.2 and 0.3 μm, well before the closure of the inner membrane, indicating that it is not engaged in the late stage of division.[34,35] Thus, the final stage of septation in vivo is achieved by mechanisms not involving FtsZ, possibly peptidoglycan biosynthesis pushing the inner membrane[33] and/or excess membrane synthesis.[36,37]

Importantly, GUVs have been instrumental to investigate bacterial division proteins and many other membrane processes. However, while they mimic some of the features of cellular membranes, they admittedly lack a number of physiological characteristics, such as the molecular diversity (both lipids and proteins), mechanical properties, size and spontaneous curvature that most likely play an important role in proto-ring organization. Therefore, conclusions drawn from GUV-based assays provide new hypotheses that need to be validated by in vivo experiments.

Combining the latest in vivo observations and the present results, the prospect of achieving robust liposome fission with the mere bacterial division proteins FtsA and FtsZ is rapidly fading. Although genetically controlled synthesis of FtsA and FtsZ can reliably re-shape liposomes into a morphology featuring an increase in both the surface-to-volume ratio and membrane curvature, it becomes evident that assisting mechanisms, either programmed in a synthetic genome or relying on external factors (or a combination thereof) will be necessary for final abscission. We hereafter propose several possible strategies:

1) Compartmentalized gene-based synthesis and self-organization of division proteins enables function optimization through in vitro evolution strategies (**Figure 6**a). Activity improvement may arise from fine-tuning the absolute and relative amounts of the encoded proteins, or optimization of their properties. Rounds of genetic diversification, along with selection of liposomes displaying a desirable phenotype, such as dumbbell-shaped constricted liposomes with a fissionable membrane neck, would enrich the population of liposomes equipped with an improved division apparatus. Balancing the effective concentration of proteins is essential for in vivo cell division. Small differences in the amounts of key cell division players can have a significant impact on cell proliferation.[38,39] Throughout the cell cycle, a complex collection of regulatory elements, comprising growth rate-mediated signaling, antisense RNAs, and effector proteins, guarantees that adequate amounts of division proteins are produced at a specific time.[40] Therefore, control over gene expression levels in liposomes may increase the rate of functionally assembled Z-rings. This could be achieved by modulating the strength of transcription and translation of the individual genes, for instance, through mutagenesis of regulatory DNA sequences (Figure 6a), or by adjusting the PURE composition and expression conditions (Figure 6b). Moreover, evolutionary engineering of FtsZ and FtsA may accelerate the discovery of new mutants that enable liposome splitting.
2) Engineering temporal control over gene expression might also be necessary for timing the self-organization events underlying division (Figure 6c). In vivo example of temporal control at the genetic level is the observation that transcriptional activity of *ftsZ* rises during the cell cycle, with an increase in FtsZ production correlating with the appearance of the Z-ring.[41–43]
3) Z-ring-constricted liposomes provide a scaffold to integrate additional factors that may aid in completing division.[44] Such elements include FtsN, Zap-family proteins, as well as MinC and ClpXP for disassembling FtsZ filaments (Figure 6d).
4) Division necessitates an increase in the area-to-volume ratio,[45] something that an elongated shape would favor. Elongation is often the initial stage towards binary fission, followed by membrane invagination. Reconstituting an entire elongation complex as found in *E. coli* is probably not the way to go.[46–48] Alternatively, cell-free expression of bacterial microtubules has been found to elongate liposomes,[49] and could be integrated to the FtsA-FtsZ system (Figure 6e).
5) Non-protein-based approaches should be explored to overcome the energy barrier associated to fission. The dramatic membrane remodeling induced by adding 100×10^{-3} M sucrose in the external environment widened up the necks instead of encouraging septum formation and division (Figure 3b). It should be noted that at such concentrations, sucrose can bind to the membrane,[50] increasing the mean surface area per lipid, hence the vesicle surface-to-volume ratio. The increased thermal fluctuations of the expanded membrane might create forces in the opposite direction than those exerted by FtsZ. The use of different osmolytes, such as monovalent ions, divalent cations, and monosaccharides known to have a low affinity to membranes,[50] as well as the use of enzymatic method to gradually change osmolarity[51] should be investigated (Figure 6f). As discussed above in the context of peptidoglycan/membrane synthesis-coupled division in bacteria, phospholipid biosynthesis within liposomes[52,53] or excess membrane from external supply of lipids may promote formation of a septum at the constriction sites (Figure 6g). This approach would benefit from using composite membranes with varying lipid shapes and chain lengths that are prone to alter liposome morphology and membrane tension[54–57] (Figure 6h). Furthermore, the two leaflets of the liposome membrane could be asymmetrically modified to increase the line tension and spontaneous curvature (Figure 6i). This could be achieved using the photosensitizer Chlorin e6, which causes local lipid peroxidation upon illumination over a time scale of minutes.[58]
6) Finally, mechanical perturbations, such as gentle shear forces or sonication, may also elicit division events at the membrane neck of constricted liposomes (Figure 6j), a scenario that may have been important in the development of early life before full genetic control.[59]

The combined action of genetically encoded division proteins and external stimuli (e.g., temperature cycling, osmolyte or lipid addition, mechanical perturbations) will result in a semi-autonomous mode of division. Integration of the missing functions into the DNA program will eventually increase the level of autonomy.[60]

© 2023 The Authors. Advanced Biology published by Wiley-VCH GmbH

27010198, 0, Downloaded from https://onlinelibrary.wiley.com/doi/10.1002/adbi.202200172 by Tu Delft, Wiley Online Library on [09/01/2023]. See the Terms and Conditions (https://onlinelibrary.wiley.com/terms-and-conditions) on Wiley Online Library for rules of use; OA articles are governed by the applicable Creative Commons License

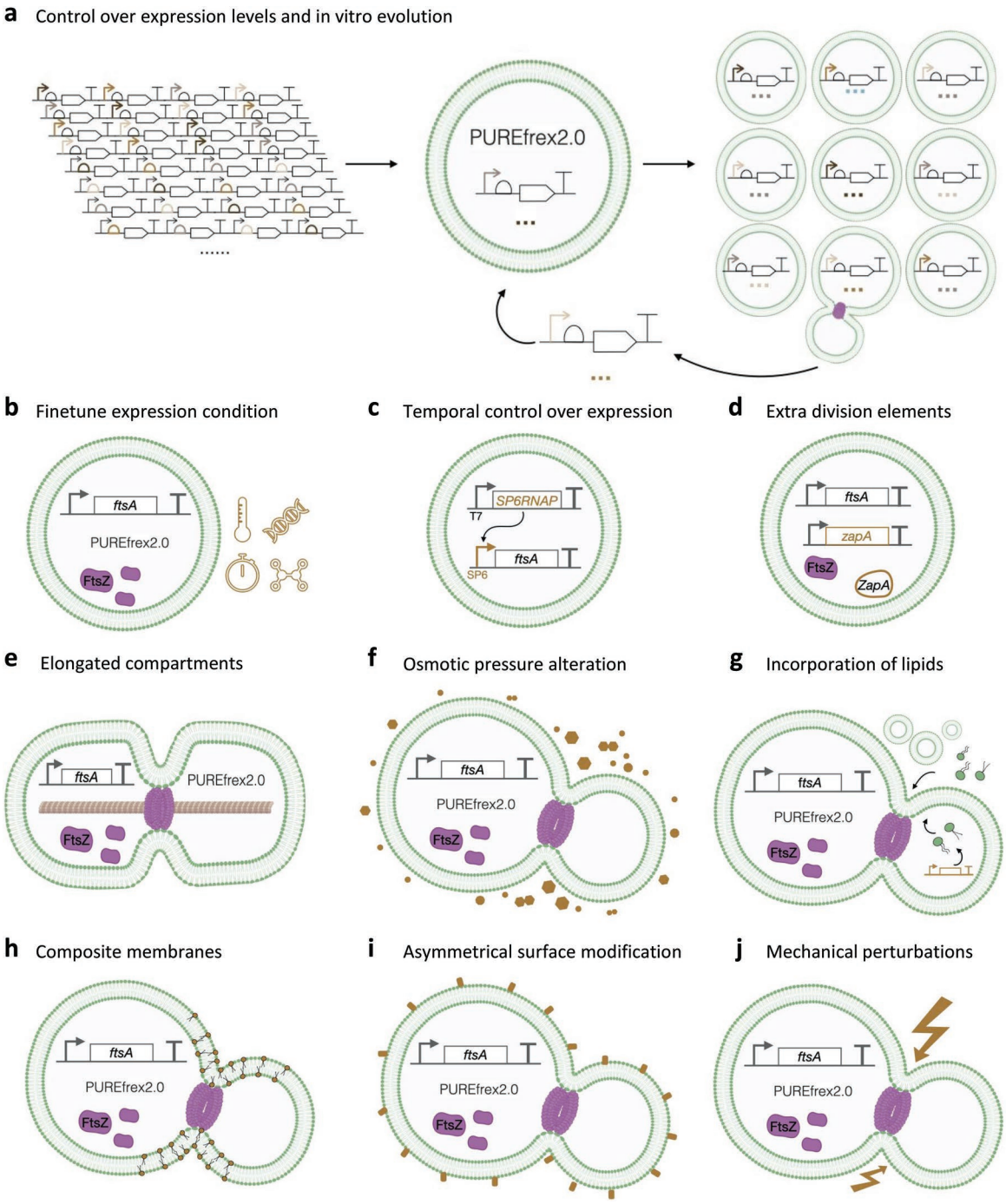

Figure 6. Possible strategies for assisting FtsA-FtsZ in dividing liposomes. a) Control over the abundance of expressed proteins can be achieved by designing a DNA library of regulatory elements (e.g., promoters, ribosome binding site, transcription terminator). Single variants from the DNA pool and PURE system are co-encapsulated within liposomes. Upon gene expression, the few liposomes exhibiting a desirable phenotype are selected and the DNA content extracted to start a new round of the directed evolution cycle. Such an evolutionary approach can also be used to engineer mutants of FtsA or/and FtsZ empowered with the ability to divide liposomes. b) Optimization of protein synthesis by varying the molecular composition (e.g., concentration of genes, PURE components, chaperones) and the incubation conditions (e.g., temperature and time). c) Introducing temporal control over gene expression for timing the sequence of molecular events involved in division. An example of gene network designed for delayed expression is depicted. d) Addition of other factors implicated in *E. coli* cytokinesis (FtsN and Zap proteins). e) Elongation of liposomes by cell-free expression of bacterial microtubules or through external stimuli, such as electric fields and thermal expansion. f) Increase of the liposome area-to-volume ratio by external addition of osmolytes. g) Membrane expansion via the incorporation of lipids that are either internally produced by gene-encoded enzymes or directly supplied in the external environment. h) Composite membranes with different lipid shapes and chain lengths can affect liposome membrane tension and spontaneous curvature. i) Expansion differential between the two bilayer leaflets, for instance via asymmetric binding of an external molecule, can promote division through an increase of the line tension and spontaneous curvature. j) Mechanical perturbations (e.g., gentle shear forces or sonication) of pre-constricted liposomes may disrupt the membrane neck.

© 2023 The Authors. Advanced Biology published by Wiley-VCH GmbH

27010198, 0, Downloaded from https://onlinelibrary.wiley.com/doi/10.1002/adbi.202200172 by Tu Delft, Wiley Online Library on [09/01/2023]. See the Terms and Conditions (https://onlinelibrary.wiley.com/terms-and-conditions) on Wiley Online Library for rules of use; OA articles are governed by the applicable Creative Commons License

4. Experimental Section

DNA Constructs: The *ftsA* construct (starting with a T7 promoter and ending with the T7 terminator) was sequence-optimized for codon usage, GC content and 5′ mRNA secondary structures, and was inserted in a pUC57 plasmid (GeneScript). *E. coli* TOP10 competent cells were transformed with the plasmid by heat shock. Plasmid purification was performed using the PureYield Plasmid Miniprep System (column method, Promega). Concentration and purity of the isolated DNA were checked using a ND-1000 UV-Vis Spectrophotometer (Nanodrop Technologies).

The *ftsA** (FtsA_R286W) template was constructed by site-directed mutagenesis PCR using the *ftsA*-containing plasmid as a template with primers 1279 ChD and 1280 ChD (Table S1, Supporting Information). The PCR product was checked on a 1% agarose gel stained with SYBR safe, imaged with a ChemiDoc Imaging System (BioRad Laboratories), and purified with the Wizard SV Gel kit (Promega). The purified DNA was incubated with DpnI (New England BioLabs) to remove residual plasmid and the linear DNA was purified again with Wizard SV Gel kit. DNA concentration and purity were measured with a Nanodrop. *E. coli* DH5α competent cells were transformed by heat shock. Cells were centrifuged, resuspended in 50 µL of fresh prechilled liquid lysogeny broth (LB) medium and incubated for 1 h at 37 °C and 250 rpm. The cultures were plated on solid LB medium with ampicillin and grown overnight at 37 °C. Plasmid purification was performed using the PureYield Plasmid Miniprep System. Plasmid concentration and purity were checked on a Nanodrop. DNA sequence was confirmed by Sanger sequencing.

Linear templates for PURE system reactions were prepared by PCR using the *ftsA*- or *ftsA**-containing plasmid as template with primers 709 ChD and 757 ChD (Table S1, Supporting Information). Amplification products were checked on a 1% agarose gel and purified using the Wizard SV Gel kit. DNA concentration and purity were measured with a Nanodrop. The sequences of the two linearized constructs can be found in the Supporting Information.

Purified Protein: Labeled purified FtsZ was prepared as previously described[61] and was stored in 50×10^{-3} M Tris, 500×10^{-3} M KCl, 5×10^{-3} M $MgCl_2$, and 5% glycerol at pH 7.

Lipids: 1,2-Dioleoyl-sn-glycero-3-phosphocholine (DOPC), 1,2-dioleoyl-sn-glycero-3phosphoglycerol (DOPG), and 1,2-distearoyl-sn-glycero-3-phosphoethanolamine-N-[biotinyl(polyethylene glycol)-2000 (DSPE-PEG-biotin), were from Avanti Polar Lipids. Texas Red 1,2-dihexadecanoyl-sn-glycero-3-phosphoethanolamine (DHPE-TexasRed) was from Invitrogen. All lipids were purchased dissolved in chloroform.

Production of Lipid-Coated Beads: Glass beads were coated with a lipid film according to a published protocol.[11] Briefly, 5 mg of lipids in chloroform consisting of DOPC (75 mol%), DOPG (25 mol%), DSPE-PEG-biotin (1 mass%), and DHPE-TexasRed (0.5 mass%) was poured in a round-bottom glass flask. Methanol containing 100×10^{-3} M rhamnose (Sigma Aldrich) was added at a chloroform-to-methanol volume ratio of 2.5:1. Glass beads with a diameter of 212–300 µm (acid washed, Sigma Aldrich) and a total mass of 1.5 g were added to the lipid-rhamnose solution, the chloroform was removed by rotary evaporation at 200 mbar for 2 h at room temperature, followed by overnight desiccation. The lipid-coated beads were aliquoted in Eppendorf tubes and kept under argon at −20 °C. The lipid composition used here does not include cardiolipin and DOPE in contrast to a previous study.[11] This new composition led to a higher percentage of liposomes with the phenotypes of interest.

Preparation of the Imaging Chambers: Three microscopy glass slides were glued together with NOA 61 glue (Norland Products) and drilled over to produce 2.5 mm diameter holes. To create the bottom of the chamber, a 150-µm thick coverslip (Menzel-Gläser) was bonded to one side with NOA glue. Chambers were washed in a bath sonicator (Sonorex Digitec, Bandelin) by sequential steps of 10 min each using the following solutions: chloroform and methanol (volume 1:1), 2% Hellmanex, 1 M KOH, 100% ethanol, and MilliQ water. Before an experiment, the surface of the imaging chamber was functionalized with Neutravidin for liposome immobilization, as previously described.[11]

Cell-Free Gene Expression and Liposome Formation: PURE*frex*2.0 (GeneFrontier Corporation, Japan) was utilized in 20-µL reaction volumes following the instructions provided by the supplier. The linear DNA template was used at a final concentration of 5×10^{-9} M. The solution was supplemented with 1 µL DnaK Mix (GeneFrontier Corporation), SUPERase•In RNase Inhibitor (0.75 U µL^{-1} final, Invitrogen), 2×10^{-3} M GTP, 2×10^{-3} M ATP, 3×10^{-6} M FtsZ-A647 and mixed with about 20 mg of lipid-coated beads. RNase inhibitor was supplemented as a modification of the previous protocol and was shown to increase the number of liposomes with FtsA-FtsZ structures. For experiments where gene expression occurred outside liposomes, a PURE*frex*2.0 solution was assembled as described above, except that DNA and FtsZ-A647 were omitted. Liposomes were formed by spontaneous swelling of the lipid film for 45 min while tumbling at 4 °C in a cold room, protected from light. This was a protocol adjustment to optimize time management and overall sample quality. Four freeze–thaw cycles were then applied by dipping the sample into liquid nitrogen and thawing on ice. About 7 µL of the liposome solution was carefully pipetted (with a cut tip) into the imaging chamber and supplemented with RQ1 DNase (0.07 U µL^{-1}) to inhibit gene expression outside liposomes. For the assays where FtsA was produced outside liposomes, the *ftsA* gene and FtsZ-A647 were supplied in the external solution and addition of DNase was omitted. The chamber was sealed by sticking a 20×20 mm coverslip with a double-sided adhesive silicone sheet and mounted on the microscope stage. Expression was performed directly on the confocal microscope at 37 °C for 3–6 h. In the experiments with osmolarity differential, 100 or 200×10^{-3} M sucrose were carefully pipetted in the imaging chamber after 3 h of gene expression. First, a solution of sucrose (2 M stock concentration) was prepared in an equivalent osmolarity buffer as PURE system (about 800 mOsmol L^{-1}). Either 0.35 or 0.7 µL of the sucrose solution was pipetted in the liposome imaging chamber (final volume of about 7 µL) to reach a final concentration of 100 or 200×10^{-3} M sucrose, respectively.

Labeling of Synthesized Proteins and Gel Analysis: PURE*frex*2.0 reaction mixture was supplemented with 0.5 µL of GreenLys reagent (FluoroTect GreenLys, Promega). Gene expression was carried out in a test tube for 3 h at 37 °C. Proteins were denatured in 2× SDS loading buffer with 10×10^{-3} M dithiotreitol (DTT) for 10 min at 90 °C. Samples were loaded on a 18% SDS-PAGE gel. Cell-free expressed fluorescently labeled proteins were visualized using a fluorescence gel imager (Typhoon, Amersham Biosciences) with a 488 nm laser and a 520 nm band-pass emission filter.

Confocal Microscopy and Image Analysis: Liposomes were imaged using a Nikon A1R Laser scanning confocal microscope equipped with an SR Apo TIRF 100 oil immersion objective. The membrane dye (Texas Red) and FtsZ-A647 were imaged using the 561 and 640 nm laser lines, respectively, with appropriate emission filters. The NIS (Nikon) program was used for image acquisition with identical settings for all experiments. While acquiring the images, samples were kept at 37 °C in a temperature-controlled stage. Fiji[62] was used for calculating the apparent length of the membrane necks and the liposome diameters.

Statistical Analysis: All the experiments discussed in this report were replicated, and identical findings were obtained. Microscopy images are representative of the analyzed samples across at least three independent biological replicates. Data are presented as mean ± standard deviation and the sample size is indicated in the figure legends.

Supporting Information

Supporting Information is available from the Wiley Online Library or from the author.

Acknowledgements

The authors are grateful to Ilja Westerlaken for preparing the *ftsA** template and to Germán Rivas for providing purified FtsZ-A647.

© 2023 The Authors. Advanced Biology published by Wiley-VCH GmbH

27010198, 0, Downloaded from https://onlinelibrary.wiley.com/doi/10.1002/adbi.202200172 by Tu Delft, Wiley Online Library on [09/01/2023]. See the Terms and Conditions (https://onlinelibrary.wiley.com/terms-and-conditions) on Wiley Online Library for rules of use; OA articles are governed by the applicable Creative Commons License

Microscopy measurements were carried out at the Kavli Nanolab Imaging Center Delft. This work was founded by the Netherlands Organization for Scientific Research (NWO/OCW) via the "BaSyC – Building a Synthetic Cell" Gravitation grant (024.003.019).

Conflict of Interest

The authors declare no conflict of interest.

Author Contributions

E.G. and C.D. designed the experiments and wrote the paper. E.G. performed the experiments and analyzed the data. Both authors discussed the results.

Data Availability Statement

The data that support the findings of this study are available from the corresponding author upon reasonable request.

Keywords

bacterial cytokinesis, bottom-up synthetic biology, cell-free gene expression, synthetic cells

Received: June 23, 2022
Revised: November 15, 2022
Published online:

[1] P. L. Luisi, *Anat. Rec.* **2002**, *268*, 208.
[2] P. L. Luisi, T. Oberholzer, A. Lazcano, *Helv. Chim. Acta* **2002**, *85*, 1759.
[3] T. Oberholzer, P. L. Luisi, *J Biol Phys* **2002**, *28*, 733.
[4] P. L. Luisi, F. Ferri, P. Stano, *Naturwissenschaften* **2006**, *93*, 1.
[5] M. Osawa, D. E. Anderson, H. P. Erickson, *Science* **2008**, *320*, 792.
[6] M. Osawa, D. E. Anderson, H. P. Erickson, *EMBO J.* **2009**, *28*, 3476.
[7] M. Osawa, H. P. Erickson, *Proc. Natl. Acad. Sci. USA* **2013**, *110*, 11000.
[8] E. J. Cabré, A. Sánchez-Gorostiaga, P. Carrara, N. Ropero, M. Casanova, P. Palacios, P. Stano, M. Jiménez, G. Rivas, M. Vicente, *J. Biol. Chem.* **2013**, *288*, 26625.
[9] P. Szwedziak, Q. Wang, T. A. M. Bharat, M. Tsim, J. Löwe, *Elife* **2014**, *3*, e04601.
[10] T. Furusato, F. Horie, H. T. Matsubayashi, K. Amikura, Y. Kuruma, T. Ueda, *ACS Synth. Biol.* **2018**, *7*, 953.
[11] E. Godino, J. N. López, I. Zarguit, A. Doerr, M. Jimenez, G. Rivas, C. Danelon, *Commun. Biol.* **2020**, *3*, 539.
[12] D. A. Ramirez-Diaz, A. Merino-Salomón, F. Meyer, M. Heymann, G. Rivas, M. Bramkamp, P. Schwille, *Nat. Commun.* **2021**, *12*, 3310.
[13] P. C. Peters, M. D. Migocki, C. Thoni, E. J. Harry, *Mol. Microbiol.* **2007**, *64*, 487.
[14] M. Jiménez, A. Martos, M. Vicente, G. Rivas, *J. Biol. Chem.* **2011**, *286*, 11236.
[15] P. de Boer, R. Crossley, L. Rothfield, *Nature* **1992**, *359*, 254.
[16] D. RayChaudhuri, J. T. Park, *Nature* **1992**, *359*, 251.
[17] A. Mukherjee, K. Dai, J. Lutkenhaus, *Proc. Natl. Acad. Sci. USA* **1993**, *90*, 1053.
[18] K. H. Huang, J. Durand-Heredia, A. Janakiraman, *J. Bacteriol.* **2013**, *195*, 1859.
[19] D. Bramhill, C. M. Thompson, *Proc. Natl. Acad. Sci. USA* **1994**, *91*, 5813.
[20] H. P. Erickson, D. W. Taylor, K. A. Taylor, D. Bramhill, *Proc. Natl. Acad. Sci. USA* **1996**, *93*, 519.
[21] M. A. Oliva, S. Huecas, J. M. Palacios, J. Martín-Benito, J. M. Valpuesta, J. M. Andreu, *J. Biol. Chem.* **2003**, *278*, 33562.
[22] A. Mukherjee, J. Lutkenhaus, *J. Bacteriol.* **1994**, *176*, 2754.
[23] S. Pichoff, J. Lutkenhaus, *EMBO J.* **2002**, *21*, 685.
[24] B. Geissler, D. Elraheb, W. Margolin, *Proc. Natl. Acad. Sci. USA* **2003**, *100*, 4197.
[25] D. A. Ramirez-Diaz, D. A. García-Soriano, A. Raso, J. Mücksch, M. Feingold, G. Rivas, P. Schwille, *PLoS Biol.* **2018**, *16*, e2004845.
[26] Y. Shimizu, A. Inoue, Y. Tomari, T. Suzuki, T. Yokogawa, K. Nishikawa, T. Ueda, *Nat. Biotechnol.* **2001**, *19*, 751.
[27] Y. Shimizu, T. Kanamori, T. Ueda, *Methods* **2005**, *36*, 299.
[28] K. A. Ganzinger, A. Merino-Salomón, D. A. García-Soriano, A. N. Butterfield, T. Litschel, F. Siedler, P. Schwille, *Angew. Chem., Int. Ed.* **2020**, *59*, 21372.
[29] M. Krupka, V. W. Rowlett, D. Morado, H. Vitrac, K. Schoenemann, J. Liu, W. Margolin, *Nat. Commun.* **2017**, *8*, 15957.
[30] S. Pichoff, B. Shen, B. Sullivan, J. Lutkenhaus, *Mol. Microbiol.* **2012**, *83*, 151.
[31] D. Blanken, P. van Nies, C. Danelon, *Phys. Biol.* **2019**, *16*, 045002.
[32] A. I. Rico, M. Krupka, M. Vicente, *J. Biol. Chem.* **2013**, *288*, 20830.
[33] C. Coltharp, J. Buss, T. M. Plumer, J. Xiao, *Proc. Natl. Acad. Sci. USA* **2016**, *113*, E1044.
[34] B. Söderström, K. Mirzadeh, S. Toddo, G. von Heijne, U. Skoglund, D. O. Daley, *Mol. Microbiol.* **2016**, *101*, 425.
[35] B. Söderström, K. Skoog, H. Blom, D. S. Weiss, G. von Heijne, D. O. Daley, *Mol. Microbiol.* **2014**, *92*, 1.
[36] R. Mercier, Y. Kawai, J. Errington, *Cell* **2013**, *152*, 997.
[37] M. Osawa, H. P. Erickson, *Front. Microbiol.* **2018**, *9*, 111.
[38] K. Dai, J. Lutkenhaus, *J. Bacteriol.* **1992**, *174*, 6145.
[39] S. J. Dewar, K. J. Begg, W. D. Donachie, *J. Bacteriol.* **1992**, *174*, 6314.
[40] S. J. Dewar, R. Dorazi, *FEMS Microbiol. Lett.* **2000**, *187*, 1.
[41] Q. M. Yi, S. Rockenbach, J. E. Ward, J. Lutkenhaus, *Mol. Biol.* **1985**, *184*, 399.
[42] S. J. Dewar, V. Kagan-Zur, K. J. Begg, W. D. Donachie, *Mol. Microbiol.* **1989**, *3*, 1371.
[43] J. Männik, B. E. Walker, J. Männik, *Mol. Microbiol.* **2018**, *110*, 1030.
[44] N. Baranova, P. Radler, V. M. Hernández-Rocamora, C. Alfonso, M. López-Pelegrín, G. Rivas, W. Vollmer, M. Loose, *Nat. Microbiol.* **2020**, *5*, 407.
[45] H. G. Döbereiner, J. Käs, D. Noppl, I. Sprenger, E. Sackmann, *Biophys. J.* **1993**, *65*, 1396.
[46] T. Den Blaauwen, M. A. de Pedro, M. Nguyen-Distèche, J. A. Ayala, *FEMS Microbiol. Rev.* **2008**, *32*, 321.
[47] P. Szwedziak, J. Löwe, *Curr. Opin. Microbiol.* **2013**, *16*, 745.
[48] R. van der Ploeg, J. Verheul, N. O. E. Vischer, S. Alexeeva, E. Hoogendoorn, M. Postma, M. Banzhaf, W. Vollmer, T. den Blaauwen, *Mol. Microbiol.* **2013**, *87*, 1074.
[49] J. Kattan, A. Doerr, M. Dogterom, C. Danelon, *ACS Synth. Biol.* **2021**, *10*, 10.
[50] H. D. Andersen, C. Wang, L. Arleth, G. H. Peters, P. Westh, *Proc. Natl. Acad. Sci. USA* **2011**, *108*, 1874.
[51] Y. Dreher, K. Jahnke, E. Bobkova, J. P. Spatz, K. Göpfrich, *Angew. Chem., Int. Ed. Engl.* **2021**, *60*, 10661.
[52] A. Scott, M. J. Noga, P. de Graaf, I. Westerlaken, E. Yildirim, C. Danelon, *PLoS One* **2016**, *11*, e0163058.
[53] D. Blanken, D. Foschepoth, A. C. Serrão, C. Danelon, *Nat. Commun.* **2020**, *11*, 4317.
[54] M. Traïkia, D. E. Warschawski, O. Lambert, J. L. Rigaud, P. F. Devaux, *Biophys. J.* **2002**, *83*, 1443.

© 2023 The Authors. Advanced Biology published by Wiley-VCH GmbH

27010198, 0, Downloaded from https://onlinelibrary.wiley.com/doi/10.1002/adbi.202200172 by Tu Delft, Wiley Online Library on [09/01/2023]. See the Terms and Conditions (https://onlinelibrary.wiley.com/terms-and-conditions) on Wiley Online Library for rules of use; OA articles are governed by the applicable Creative Commons License

[55] T. Tanaka, R. Sano, Y. Yamashita, M. Yamazaki, *Langmuir* **2004**, *20*, 9526.
[56] Y. Inaoka, M. Yamazaki, *Langmuir* **2006**, *23*, 720.
[57] M. Andes-Koback, C. D. Keating, *J. Am. Chem. Soc.* **2011**, *133*, 9545.
[58] Y. Dreher, K. Jahnke, M. Schröter, K. Göpfrich, *Nano Lett.* **2021**, *21*, 5952.
[59] C. Hentrich, J. W. Szostak, *Langmuir* **2014**, *30*, 14916.
[60] P. van Nies, I. Westerlaken, D. Blanken, M. Salas, M. Mencía, C. Danelon, *Nat. Commun.* **2018**, *9*, 1583.
[61] J. M. González, M. Jiménez, M. Vélez, J. Mingorance, J. M. Andreu, M. Vicente, G. Rivas, *J. Biol. Chem.* **2003**, *278*, 37664.
[62] C. T. Rueden, J. Schindelin, M. C. Hiner, B. E. DeZonia, A. E. Walter, E. T. Arena, K. W. Eliceiri, *BMC Bioinf.* **2017**, *18*, 529.

© 2023 The Authors. Advanced Biology published by Wiley-VCH GmbH

27010198, 0, Downloaded from https://onlinelibrary.wiley.com/doi/10.1002/adbi.202200172 by Tu Delft, Wiley Online Library on [09/01/2023]. See the Terms and Conditions (https://onlinelibrary.wiley.com/terms-and-conditions) on Wiley Online Library for rules of use; OA articles are governed by the applicable Creative Commons License